Volume 5 | Number 9 | 7 March 2017 | Pages 2191–2476

Journal of Materials Chemistry C

Materials for optical, magnetic and electronic devices

rsc.li/materials-c

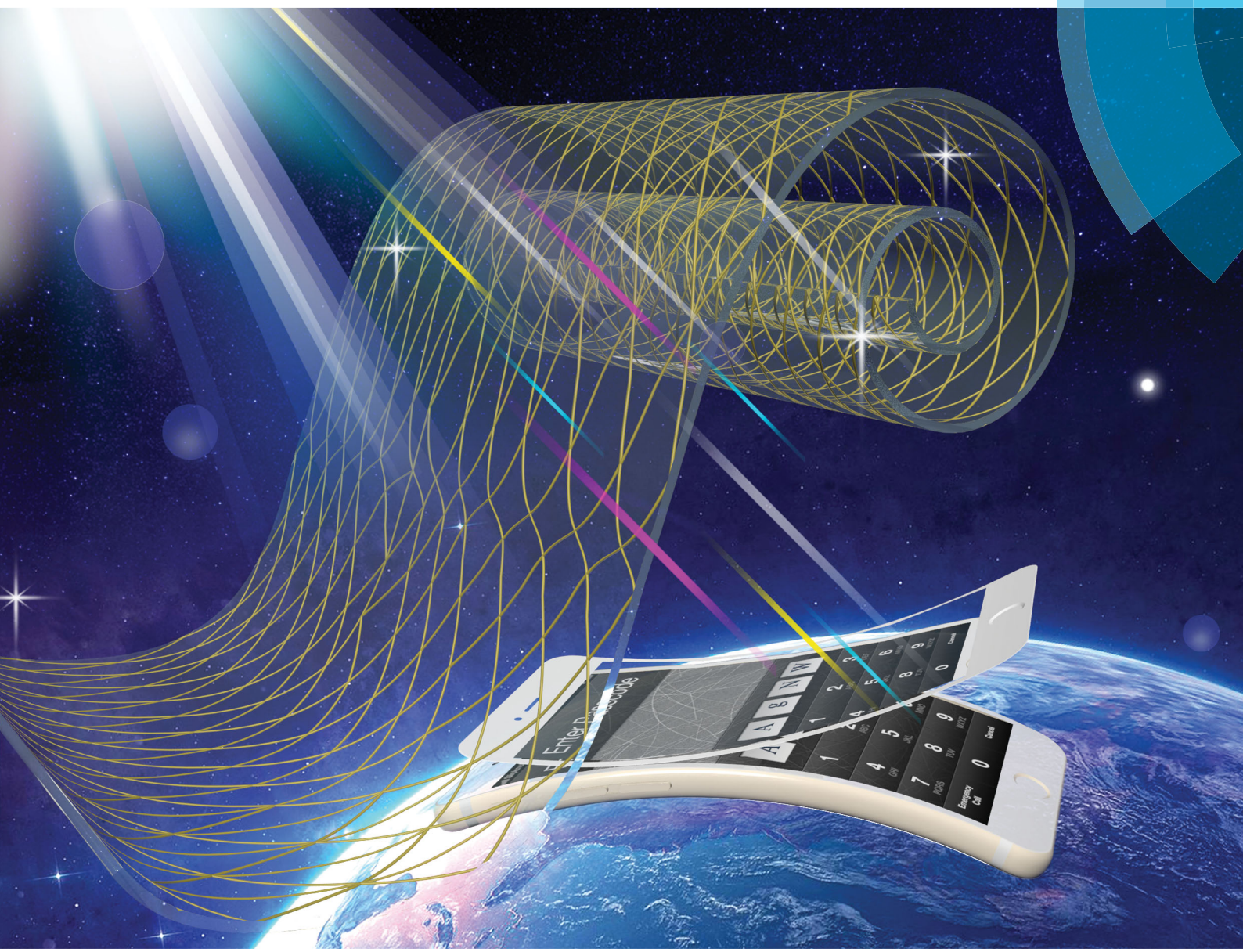

ISSN 2050-7526

ROYAL SOCIETY OF CHEMISTRY

PAPER

Shulin Ji, Changhui Ye *et al.*

Fabrication of silver nanowire transparent conductive films with an ultra-low haze and ultra-high uniformity and their application in transparent electronics

Published on 31 January 2017. Downloaded by Hefei Institutes of Physical Science, Chinese Academy of Sciences on 7/18/2018 8:29:28 AM.

Journal of Materials Chemistry C

PAPER

View Article Online
View Journal | View Issue

Cite this: J. Mater. Chem. C, 2017, 5, 2240

Fabrication of silver nanowire transparent conductive films with an ultra-low haze and ultra-high uniformity and their application in transparent electronics†

Chao Chen,[ab] Yan Zhao,[c] Wei Wei,[c] Jingqi Tao,[ab] Guowei Lei,[c] Dan Jia,[ab] Mengjuan Wan,[ab] Shuxin Li,[a] Shulin Ji*[a] and Changhui Ye*[a]

Received 18th December 2016,
Accepted 31st January 2017

DOI: 10.1039/c6tc05455b

rsc.li/materials-c

Silver nanowire transparent conductive films are one of the most promising alternatives to indium tin oxide films in the application of touch panels. Low haze and high uniformity are two essential factors for high-end applications of the films. However, the reported haze and uniformity of such kinds of films are still lagging much behind what is required for real-world applications. Herein, the fabrication of silver nanowire transparent conductive films with an ultra-low haze and ultra-high uniformity is reported. DLVO theory is applied to purify silver nanowires and the corresponding ink of the nanowires with narrower size dispersion and less nanoparticle contaminants is formulated for film coating. The fabricated films exhibit a low haze of 0.8% and good uniformity with the non-uniformity factor of 5.0% (defined as the standard deviation of the sheet resistance) at a transmittance of 91.7% (99.4% for the silver nanowire network only without a substrate) and a sheet resistance of 71.2 Ω square^{-1}. The outperforming films are utilized to construct touch-panels with excellent performance for fluent writing. The findings in this work will pave the way for real-world applications of silver nanowire transparent conductive films replacing those of indium tin oxide.

Introduction

Silver nanowire (AgNW) transparent conductive films (TCFs) have attracted enormous research attention as building blocks for large-area touch screens, thin film solar cells, organic light emitting diodes and flexible heaters.[1–14] It has been theoretically and experimentally demonstrated that TCFs composed of thin and long AgNWs are conducive to the applications that require a low haze.[15–18] As a result, there have been many reports on the synthesis of ultra-thin AgNWs by a polyol method in recent years. For instance, Sun *et al.* demonstrated an effective method to synthesize uniform AgNWs with an average diameter of 30 nm using platinum nanoparticles as seeds to direct the growth of AgNWs.[19] Lee *et al.* proposed a brief route to regulate the diameter of AgNWs in a range of 15–22 nm utilizing a high pressure polyol method.[20] Hu *et al.* decreased the diameter of AgNWs by introducing bromide ions in the precursor solution.[21] More recently, Li *et al.* produced AgNWs with an average diameter of 20 nm and an aspect ratio over 2000 when both NaBr and NaCl were introduced in the precursor solution.[22] Silva *et al.* used the single halide of NaBr with appropriate concentration and slow injection of $AgNO_3$ to synthesize AgNWs with a diameter of ~20 nm after short time termination of the reaction.[23] Unfortunately, thin AgNWs synthesized by the polyol method are always accompanied by nanoparticles (NPs) and nanorods (NRs) as the side products; in addition, the as-synthesized nanowires are typically of a large dispersion diameter, dramatically increasing the haze and worsening the uniformity of TCFs.[24,25]

Efforts have been devoted to improving the purity of AgNWs through removal of the undesirable NPs. Purification methods could be divided into the following main categories: centrifugation,[19,26–28] ordinary filtration,[29,30] cross-flow filtration,[25] decantation,[2] acetone cleaning,[22,27,28] and others. High speed or long duration of centrifugation is often applied to discard excess surfactant of polyvinylpyrrolidone (PVP) or small NPs depending on product conditions; however, it is difficult to balance between the purification effect and dispersibility of AgNWs in the latter procedure of ink formulation. It requires much time for ordinary filtration without pressure assistance

[a] Key Laboratory of Materials Physics and Anhui Key Laboratory of Nanomaterials and Technology, Institute of Solid State Physics, Chinese Academy of Sciences, Hefei 230031, China. E-mail: slji@issp.ac.cn, chye@issp.ac.cn
[b] University of Science and Technology of China, Hefei 230026, China
[c] Shaanxi Coal and Chemical Technology Institute Co. Ltd, Shaanxi Xian 710065, China

† Electronic supplementary information (ESI) available: Photographs of experimental devices and products, additional SEM images, optical curves, schematic diagrams and one video. See DOI: 10.1039/c6tc05455b

This journal is © The Royal Society of Chemistry 2017

Published on 31 January 2017. Downloaded by Hefei Institutes of Physical Science, Chinese Academy of Sciences on 7/18/2018 8:29:28 AM.

Table 1 Comparison of the key properties among AgNW TCFs fabricated by various coating methods

Concentration (mg mL^{-1})	Coating method	Coating cycles	R_{Sh} (Ω $\square^{-1}$)	Haze (%)	NUF (%)	σ_{DC}/σ_{OP}	Ref.
0.5	Spray	NA	27.4	5.0	NA	127.2	31
2.5	Spray	NA	20	4.9	NA	224.4	29
4.5	Mayer rod	Many	480	2.0	NA	10.6	32
NA	Bar	Many	109	1.6	NA	112.7	33
0.5	Bar	Many	30	1.0 (with PET)	NA	200	28
0.2	Bar	6	35	NA	6.7	231.1	34
NA	Mayer rod	1	130	NA	NA	320	22
1	Automatic coating machine	1	34.5	1.0 (with PET)	6.3	772.3	This work
1	Automatic coating machine	1	71.2	0.8 (with PET)	5.0	878.5	This work

and when using a vacuum pump, dispersibility of AgNWs in the latter procedure could not be easily satisfied. Cross-flow filtration is effective in removing NPs, but it does not work so well for size dispersion control to get rid of thick NRs and short AgNWs. It is very simple to abandon small NPs by decantation, yet the difficulty in the size dispersion control of AgNWs faced by cross-flow filtration is also to be tackled. Acetone cleaning could help reduce the PVP content and size selection; nevertheless, NPs adhered tightly on the surface of AgNWs during synthesis are hard to remove solely by cleaning. The remaining NPs, the AgNWs' wide size dispersion and the poor dispersibility of AgNWs are chief factors deteriorating the optical and electrical properties of AgNW TCFs through scattering light and fluctuating sheet resistance across the film. The large haze and big non-uniformity factor of the TCFs could be anticipated. As shown in Table 1, various haze values over 1.0% of AgNW TCFs with different sheet resistances depending on nanowire size, ink composition and film formation methods were reported.[22,28,29,31–34] Most of the work did not report the uniformity; however, typical values for the standard deviation of the sheet resistance are bigger than 20%, much larger than those of indium tin oxide (ITO) films (typically in the range of 5–10%).[34] Moreover, the mechanism of interactions between reagents and Ag nanomaterials in the purification process of AgNWs is still unexplored. Thus, there is an urgent need for an effective and scalable method to separate NPs and NRs completely from AgNWs ensuring low haze and high uniformity of TCFs, even if the product is composed of nanomaterials of wide size dispersion and morphology variety.

Herein, we report a method to separate NPs and NRs absolutely from AgNW solution *via* a brief filtration and purification process. We applied the DLVO theory in colloid science to systematically investigate the mechanism of the interactions between reagents and Ag products; the fundamental physics renders the success in eliminating impurities sufficiently. We constructed TCFs using these highly purified AgNWs, and achieved a remarkably low haze of 0.8% and a distinctively small sheet resistance non-uniformity factor of 5.0% at a sheet resistance of 71.2 Ω square^{-1}.

Experimental section

Materials

$AgNO_3$ ($\geq$99.8%) was obtained from Shanghai Qiangshun Chemical Reagent Co., Ltd. Polyvinylpyrrolidone (PVP, M_W = 55 000) and hydroxypropyl methylcellulose (HPMC) were purchased from Sigma-Aldrich. Ethylene glycol (EG), NaCl, NaBr, and acetone were donated from Sinopharm Chemical Reagent Co., Ltd. Sago® 9760 and Sago® 3223 were obtained from Sago Co., Ltd. Acrylic resin as an over-coating (OC) was obtained from Guangdong Nanhai ETEB Technology Co., Ltd. All reagents were used as-received without further purification.

Synthesis of AgNWs

(A) 0.220 M NaBr, (B) 0.210 M NaCl and (C) 0.505 M PVP in EG were individually prepared for utilization. Fresh $AgNO_3$ was dissolved in EG by sonicating in an ice bath (4–8 °C) for 5 min. Subsequently 2.5 mL of A, 5 mL of B, 25 mL of C and 25 mL of $AgNO_3$ (0.265 M) were successively added to a 100 mL flask placed in an oil bath at room temperature. Vigorous stirring was applied for 30 min and then the temperature in the flask was elevated to 170 °C in 15 min, where the nitrogen gas with a flux of 150 mL min^{-1} was bubbled through the reaction. Thereafter, the flask was corked and the reaction was left for 1 h without disturbing. The flask was taken off from the oil bath immediately and transferred to the water for cooling once the reaction was terminated. Notably, this synthesis method was conducted according to a previous report.[22]

Positive-pressure filtration

The hydrophilic polytetrafluoroethylene (PTFE) membrane (diameter of 100 mm, pore size of 5 μm) dealt with 70 °C de-ionized (DI) water for 30 min was installed on a Mass-Filtration system. Polypropylene (PP) membrane (diameter of 100 mm, pore size of 10 μm) was employed as the supporting layer, preventing the PTFE membrane from destruction. 12 mL of AgNW reaction solution was dissolved in 468 mL of EG by the vortex movement of a tunable mixer (MX-S) for 3 s in a pulse form, which was subsequently transferred to the positive-pressure filtration system and filtered at the pressure of 5–20 kPa provided by the air compressor. Finally, AgNWs on the membrane was redispersed into 30 mL of 0.5 wt% PVP (M_W = 55 000) under vortex movement for 3 s, which was subsequently transferred for acetone cleaning.

AgNW cleaning with acetone

The filtered and redispersed AgNW dispersion was fixed on a rotary shaker (HY-5A) and shaken with the speed of 75 rpm, followed by titration with acetone at a rate of 100–200 μL s^{-1}. During mixing, the dispersion tends to be pale yellow

Published on 31 January 2017. Downloaded by Hefei Institutes of Physical Science, Chinese Academy of Sciences on 7/18/2018 8:29:28 AM.

indicating the flocculation of AgNWs and at that point no excess acetone should be added. After settling for 10 min, the supernatant was pipetted out, and the above procedure was recorded for 1 cycle. Thereafter, the flocculate was redispersed in 30 mL of 0.5 wt% PVP and 5–7 cycles should be conducted to remove NPs and NRs.

Formulation of stable AgNW ink

24 mL of purified AgNWs were dissolved in 16 mL of DI water with the assistance of 32 mg of HPMC, a Sago-dispersant (v/v 0.0025%) and a Sago-flatting agent (v/v 0.0025%). Finally, 1 mg mL^{-1} AgNW ink could be obtained after the mixture was fixed on a table concentrator and allowed to blend for 1.5 h with a rotating speed of 110 rpm.

Fabrication of AgNW TCFs

An automatic coating machine (BEVS 1811/2) equipped with an OSP-22 scraper was utilized to coat TCFs on polyethylene terephthalate (PET) substrates, where the coating rate and area were fixed at 100 mm s^{-1} and A4, respectively. The starting button was pressed down after dropping 1 mL of AgNW ink and TCFs were obtained after a brief annealing process at 60 °C for 5 min. A double-faced OC as an additional optical adjustment layer to reduce light scattering was employed on films of AgNWs/PET by coating acrylic resin and left at 60 °C for 1 min in a drying oven and 80 mW cm^{-2} for 1 min under UV irradiation to solidify the OC.

Characterization

The morphology of AgNWs was characterized by scanning electron microscopy (SEM) (Sirion 200 FEG) and transmission electron microscopy (TEM) (JEM-2010). Optical data were obtained on a UV-Vis-NIR spectrometer (Shimadzu SolidSpec-3600) where in all the measurements air was taken as the reference. It should be pointed out that the optical values were obtained from the entire film with the underlying substrate of PET, which has more reference value for real applications, not the case in most reports where a blank substrate was taken as the reference to give the value of AgNW networks only. The sheet resistance of TCFs was measured using a four-point probe method (RST-9, Four-Probe Tech.).

Results and discussion

The polyol method was employed to synthesize the raw AgNWs with an average diameter of 38.3 (±26.6) nm and an average length of 23.0 (±10.8) μm (Fig. 1a). In sharp contrast, purified AgNWs exhibited a much narrower dispersion with the diameter and length of 21.1 (±3.2) nm and 20.6 (±6.3) μm, respectively (Fig. 1b).

For purification of synthesized raw AgNWs, traditional methods such as centrifugation and filtration were commonly used. To accelerate the filtration rate induced merely by the gravity, a vacuum pump linked with the glass filtration system was usually applied to make use of the atmosphere pressure, which was termed as "negative-pressure filtration" here.

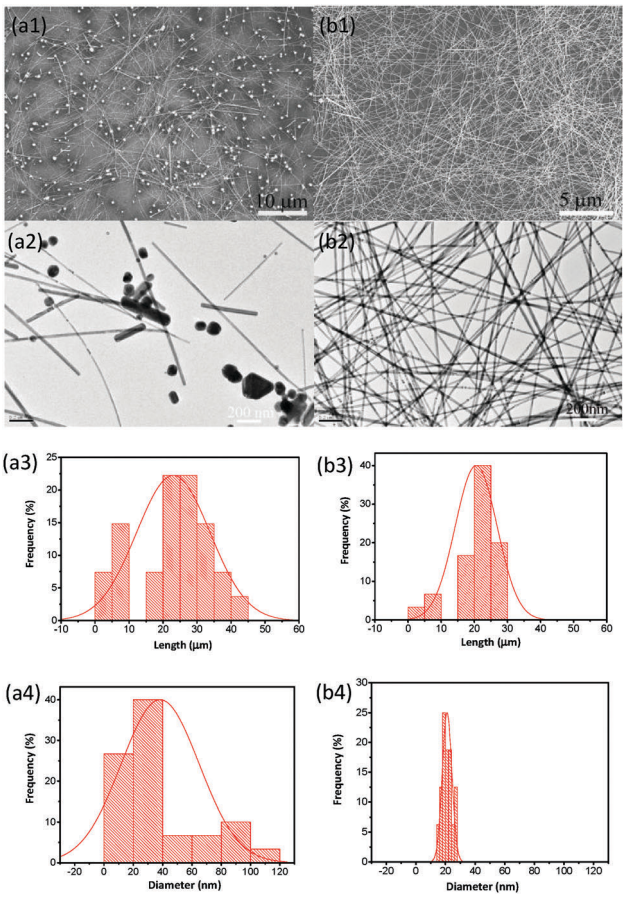

Fig. 1 (a1) SEM and (a2) TEM images, (a3) and (a4) the statistic distribution of the length and diameter of the raw AgNWs; (b1) SEM and (b2) TEM images, (b3) and (b4) the statistic distribution of the length and diameter of the purified AgNWs.

However, the differential pressure between the raw dispersion and the effluent, which depends on the vacuum degree of the glass filtration system, could not be manipulated exactly with ease (Fig. S1b, ESI†). Irreversible coagulation could be easily introduced by the unadjustable centrifugal force in the centrifugation process and overloaded pressure in the negative-pressure filtration process as shown in Fig. S1a, ESI.† In contrast, we built a "positive-pressure filtration" system using the steel device to guarantee the tightness and an air-compressor as well as two valves (one wide range followed by another fine range) to control the pressure actively imposed on the AgNW dispersion (Fig. S2, ESI†). Sophisticated pressure regulation in the range of 5–20 kPa helped to eliminate most small NPs while preventing the purified AgNWs from coagulation. It is noteworthy that the raw AgNW dispersion subjected to direct filtration was observed to contain a large amount of undesirable NPs and NRs (Fig. S3, ESI†). Considering that small NPs would be released from concentrated AgNWs when a diluent was introduced in the filtration process, we added DI water or ethylene glycol (EG) to the raw reaction solution and the results in Fig. S4, ESI† revealed that small NPs were removed more efficiently when EG was utilized as the diluent.

 This journal is © The Royal Society of Chemistry 2017

Published on 31 January 2017. Downloaded by Hefei Institutes of Physical Science, Chinese Academy of Sciences on 7/18/2018 8:29:28 AM.

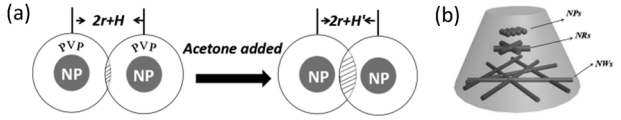

Fig. 2 (a) Schematic diagram for the osmotic pressure effect and (b) theoretical tendency towards flocculation of the AgNW dispersion after addition of a poor solvent.

After removal of most small NPs by positive-pressure filtration, DLVO theory was employed to investigate the mechanism of eliminating the undesirable remaining NPs and NRs for the subsequent acetone cleaning process.[35,36] The thickness of the diffusion layer (H) between two separate NPs capped with PVP, which was dissolved in benign solvent such as DI water, would provide a space repulsion potential energy enabling the stability of the AgNW dispersion due to the long chain branches in PVP. In contrast, H would exhibit a contraction tendency when a poor solvent such as acetone was involved, which was insoluble to PVP and would lead to the flocculation of Ag products because of the decrease of the interaction potential energy (E) according to DLVO theory (Fig. 2a):[37]

$$E = -\frac{Ar}{12H} \quad (1)$$

In the above equation, A refers to the Hamaker constant, r is the radius of NPs, and H indicates the shortest distance of the two NPs. Herein, larger NPs are more likely to flocculate than the smaller ones because they possess a larger value of $|E|$ when H was a constant. Similarly, DLVO theory could also be applied in predicting the tendency towards flocculation in platelike NRs/NWs:[38,39]

$$E_{\text{Area}} = -\frac{A}{12\pi H^2}, \quad E = -\frac{A \times \pi DL}{12\pi H^2} = -\frac{ADL}{12H^2} \quad (2)$$

Likewise, AgNWs are more readily flocculating because of the much larger length (L) than that of NRs considering the little difference in diameter (D) between long NWs and short NRs. Obviously, the tendency towards flocculation in the raw AgNW dispersion can be of the order of NWs > NRs > large NPs > small NPs when acetone was introduced (Fig. 2b and Fig. S5, ESI†).

From DLVO theory, it is easily understood in this work the key of combining positive-pressure filtration and acetone cleaning in sequence to remove both NPs and NRs and narrow the size dispersion of AgNWs. This process involved the addition of 117 mL of EG to 3 mL of reaction solution, which was further put under vortex movement for 3 s to enable excellent dispersion. Notably, vortex movement had been demonstrated as a crucial procedure enabling the mechanical separation of NPs and NRs from intertwined AgNWs (Fig. 3a). However, if excess time of vortex movement was applied, the final AgNWs were found to tend toward bending or cracking into small parts, leading to a reduction in the product yield as shown in Fig. 3c and d. After vortex movement, the mixture was filtered at 5–20 kPa to obtain AgNWs on a filtration membrane. Subsequently, 7.5 mL of 0.5 wt% PVP solution was utilized to disperse the filtered AgNWs on the filtration membrane by

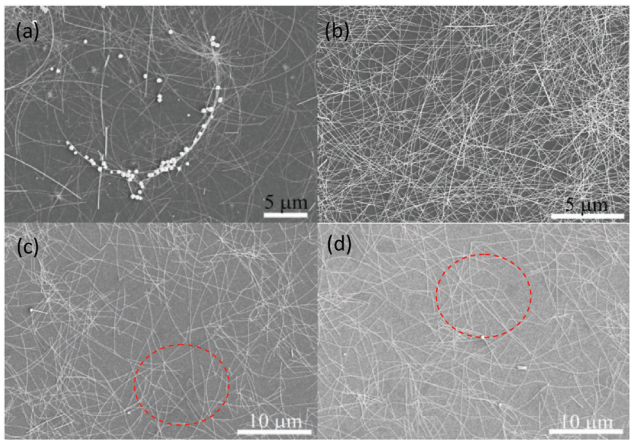

Fig. 3 SEM images of AgNWs processed with 1 cycle of positive-pressure filtration and 5 cycles of acetone cleaning when the solution of 3 mL of raw AgNWs dispersed in 117 mL of EG was put under vortex movement for (a) 0, (b) 3, (c) 7, and (d) 11 s, respectively.

putting the mixture under vortex movement for 3 s and the resultant dispersion was placed on an automatic shaker with a rotating speed of 75 rpm. During shaking, acetone was added with a dripping speed of 0.1–0.2 mL s^{-1}. The yellow floccule was formed when 20–25 mL of acetone was added, at which point dwelling for 10 min was sufficient for the separation between the floccule and the supernatant. The supernatant containing NPs and NRs was finally pipetted out. AgNWs with high purity were harvested after 5 cycles of this purification process utilizing acetone (Fig. 3b). SEM was utilized to investigate the effluent in the filtration process and the pipetted supernatant in the subsequent cleaning process with acetone after 1–5 cycles. Fig. S6a, ESI† reveals that the effluent in the filtration process was dominated by NPs. While in the pipetted supernatant, the quantity of NPs and NRs exhibited a dramatic decrease and NRs with a low aspect ratio were gradually pipetted as the purification cycles with acetone increased, which is also evidence for $|E_{\text{NWs}}| > |E_{\text{NRs}}| > |E_{\text{NPs}}|$ (Fig. S6b–f, ESI†).

Furthermore, UV-Vis measurements were carried out to investigate the quantity variation of NPs, NRs, and NWs during the purification process utilizing both filtration and acetone cleaning. The absorption peak located at 416 nm with a broad and asymmetric shape is detected from Fig. 4a, which indicates that the filtered effluent contains not only the dominant NPs but also NRs.[19,40] This broad peak greatly reduces its tail intensity as cycles of acetone cleaning increase revealing the further quick removal of NPs. It is noteworthy that the peak center gradually blue-shifted suggesting the effective removal of NRs with a smaller aspect ratio (Fig. 4b).[19,28,41–43] Finally, the absorption peak at 368 nm with a sharp and narrow shape assigned to AgNWs with a larger aspect ratio is detected from Fig. 4c for the purified product, which displays a blue-shift compared to those in Fig. 4a and b for the discarded filtered effluent and the pipetted supernatant. It demonstrates that AgNWs with high purity and narrow size distribution could be obtained through the purification process of positive-pressure filtration and acetone cleaning.[28,44,45]

Published on 31 January 2017. Downloaded by Hefei Institutes of Physical Science, Chinese Academy of Sciences on 7/18/2018 8:29:28 AM.

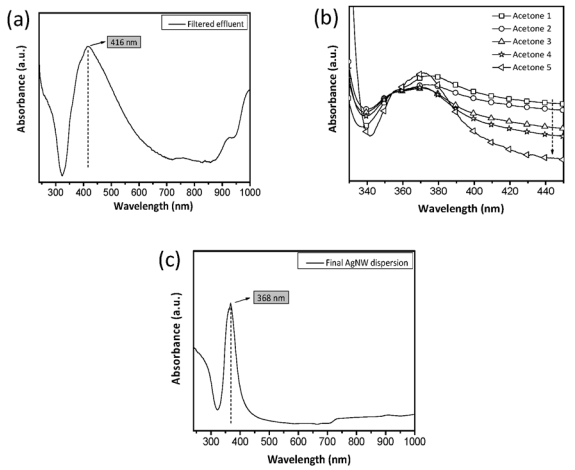

Fig. 4 UV-Vis spectra of (a) the filtered effluent, (b) the pipetted supernatant after 1–5 cycles of acetone cleaning, and (c) the final purified AgNW dispersion in ethanol.

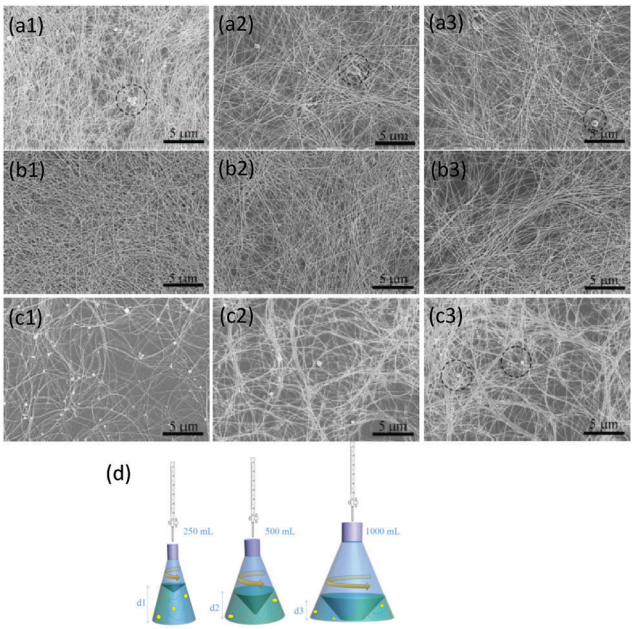

Fig. 5 SEM images of 12 mL of raw AgNW reaction solution purified by positive-pressure filtration for 1 cycle and acetone cleaning for 5–7 cycles as shown from left to right, where the acetone cleaning process was performed in a conical flask of (a) 250 mL, (b) 500 mL and (c) 1000 mL. (d) Schematic diagram showing the vortex shape and position in a conical flask with the specification of 250, 500 and 1000 mL, respectively, when acetone was added for cleaning.

The capacity of purifying up to 12 mL of raw AgNW reaction solution through 1 cycle of positive-pressure filtration and 5–7 cycles of acetone cleaning is demonstrated in Fig. 5 and Fig. S7, ESI.†

We found that for large scale AgNW purification, balancing between solution volume and the container specification to ensure the homogeneous diffusion of acetone into Ag nanomaterials by forming an appropriate vortex is of vital importance. A conical flask of 250 mL worked well for the purification of 3 mL and 6 mL of raw reaction solution by keeping the rotating speed of the automatic shaker at 75 rpm (Fig. S7a and b, ESI†). However, NPs and NRs appeared from 9 mL and 12 mL of raw reaction solution by applying the same cleaning conditions, and the impurities could still be observed as seen from Fig. S7d, ESI† though 7 cycles of acetone cleaning was performed. The disappearance of the vortex in the 250 mL conical flask leading to ineffective diffusion of acetone and unsuccessful sequential flocculation of PVP-capped AgNWs/NRs/NPs was responsible for the phenomenon. When replacing the 250 mL conical flask with a 500 mL one, the phenomenon could be eliminated and AgNWs of high purity were obtained (Fig. 5b). In addition, when using a 1000 mL conical flask to purify 12 mL of raw solution, the diffusion was inhomogeneous again during shaking due to the existence of a void at the bottom of flask, which blocked the spatial diffusion of acetone (Fig. 5c).

Shortly, we have developed an effective strategy to purify thin AgNWs synthesized with the help of Br^- and Cl^- ions by the polyol method. The strategy combines positive-pressure filtration and acetone cleaning in sequence to remove nearly all impurities of NPs (small and large) and short NRs introduced by the Br^- and Cl^- ions. Acetone cleaning alone could not achieve this goal as shown in Fig. S8, ESI.† The peeling of NPs and NRs adhered tightly on the surface of NWs in the filtration step benefits the diffusion of acetone into Ag nanomaterials and the contraction of distance between two objects for sequential flocculation of AgNWs/NRs/NPs. Exact force control during the positive-pressure filtration to prevent irreversible coagulation of AgNWs also plays an important role. The developed strategy could be applied for large scale AgNW purification if appropriate conditions are satisfied for efficient spatial diffusion of poor solvents such as acetone.

Purified AgNWs were dispersed in DI water to formulate a homogeneous ink with a concentration of 1 mg mL^{-1} under the assistance of HPMC (viscosity modifier), a Sago-dispersant (surface tension modifier) and a Sago-flatting agent (rheology modifier) as shown in Fig. 6a, which was coated on a PET substrate with the total transmittance (T_t) and haze measured as 90.8% and 1.1% at λ = 550 nm by an automatic coating machine (Fig. S9, ESI†). The TCFs were finished after installation of a double-faced over-coating (OC). According to Fig. 6b, TCFs fabricated by the purified AgNWs having a sheet resistance of 71.2 Ω $square^{-1}$ exhibited even better optical properties than those made by the raw AgNWs having a sheet resistance of 245.5 Ω $square^{-1}$. T_t was increased from 87.7% of raw AgNW TCFs to a superior value of 91.7%, and meanwhile the haze was decreased from 2.0% to the comparable value of 0.8% with that of ITO, indicating that abundant NPs existed in raw AgNWs, scattered incident light and deteriorated the optical properties.

More importantly, the homogeneous ink made from ultra-thin AgNWs with narrow size dispersion and free of NPs guaranteed the uniformity of TCFs, which was a crucial quality factor when applied on electronic devices as electrodes. The non-uniformity factor (NUF) was defined to estimate

 This journal is © The Royal Society of Chemistry 2017

Published on 31 January 2017. Downloaded by Hefei Institutes of Physical Science, Chinese Academy of Sciences on 7/18/2018 8:29:28 AM.

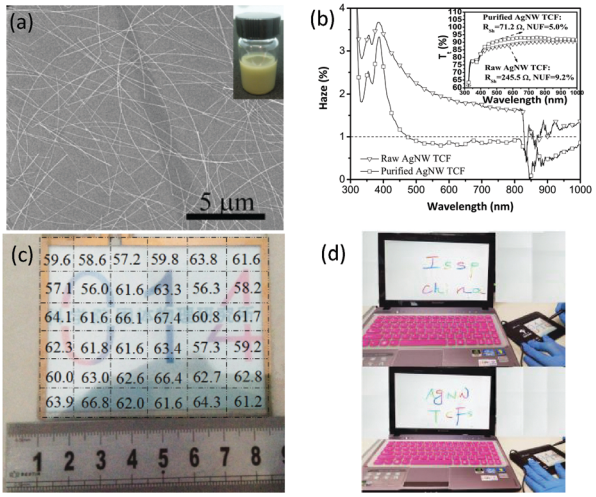

Fig. 6 (a) The formulated AgNW ink and its SEM characterization. (b) UV-Vis curves to characterize the T_t (shown in the inset) and haze of TCFs fabricated by the raw and purified AgNWs, respectively. (c) The digital picture of the AgNW TCF electrode and its sheet resistance distribution. (d) The touch-panel constructed by the AgNW TCF electrode.

the sheet resistance uniformity according to the following formula,[34]

$$\mathrm{NUF} = \sqrt{\frac{\frac{1}{N}\sum_{i=1}^{N}\left(R_i - \overline{R}\right)^2}{\overline{R}^2}}$$

where N is the number of measurements on the film of different sites, and R_i and $\overline{R}$ are the measured and average resistance of all the measurements, respectively. The smaller the NUF, the more uniform the film and the more accurate the response of devices made of the film.[34] Typically, the sheet resistance of the constructed TCFs based on the purified AgNWs had an NUF as small as 5.0%, which was much lower than that of raw AgNW TCFs (Fig. 6b, c and Fig. S10, ESI†). For comparison, a figure of merit has been widely utilized recently to exhibit the overall performance of TCFs, which is defined as the ratio of the electrical conductance to optical conductance at a wavelength of 550 nm.[46,47] The results in Table 1 demonstrates that, since being free of NPs, narrow size dispersion and uniform distribution of AgNWs, the constructed TCFs outperform most reported ones.

Regarding low sheet resistance needs, TCFs of 34.5 Ω sq^{-1} could be formed having a low haze of 1.0% and a high figure of merit of 772.

Finally, such uniform and low haze TCFs should be readily applied on the touch-panels. Fluent writing was confirmed on the constructed panels as shown in Fig. 6d (please refer to the video in the ESI†). Moreover, the device exhibited long-term stability manifesting the firm adhesion between the AgNW films and the PET substrates as well as the anti-oxidation ability of the AgNW films, which is due to the cross-linker of HPMC used in the AgNW ink,[34] and the over-coating of the acrylic resin.

Conclusions

In summary, we have demonstrated that positive-pressure filtration could enable effective removal of small NPs from raw AgNWs. Furthermore, the mechanism of size selective purification of the filtered AgNWs through acetone cleaning has been explained successfully on the basis of DLVO theory. The dispersion degree of raw reaction solution during filtration and the spatial diffusion status of acetone into nanomaterials during cleaning have been revealed as the dominating factors to affect the purity of AgNWs. Homogeneous AgNW ink has been formulated for the construction of TCFs with an ultra-low haze of 0.8% and ultra-high uniformity having an NUF of 5.0%. The purification process demonstrated here is expected to be helpful for large scale treatment of ultra-thin AgNWs for industrial applications. Finally, the construction of AgNW TCFs utilizing an automatic coating machine explored here is a promising and repeatable technique for industrial and academic researchers, seeking to produce TCFs with stable performance exceeding that of ITO.

Acknowledgements

This work was supported by the National Natural Science Foundation of China (Grant No. 51501182, 51502295, 11274308 and U1532268) and the CAS/SAFEA International Partnership Program for Creative Research Teams.

Notes and references

1 J. Lee, P. Lee, H. Lee, D. Lee, S. S. Lee and S. H. Ko, *Nanoscale*, 2012, **4**, 6408–6414.
2 C. Mayousse, C. Celle, E. Moreau, J. F. Mainguet, A. Carella and J. P. Simonato, *Nanotechnology*, 2013, **24**, 215501.
3 A. R. Madaria, A. Kumar and C. W. Zhou, *Nanotechnology*, 2011, **22**, 245201.
4 A. Kim, Y. Won, K. Woo, C. H. Kim and J. Moon, *ACS Nano*, 2013, **7**, 1081–1091.
5 M. G. Kang, T. Xu, H. J. Park, X. G. Luo and L. J. Guo, *Adv. Mater.*, 2010, **22**, 4378–4383.
6 J. Krantz, M. Richter, S. Spallek, E. Spiecker and C. J. Brabec, *Adv. Funct. Mater.*, 2011, **21**, 4784–4787.
7 C. H. Chung, T. B. Song, B. Bob, R. Zhu, H. S. Duang and Y. Yang, *Adv. Mater.*, 2012, **24**, 5499–5504.
8 D. S. Leem, A. Edwards, M. Faist, J. Nelson, D. D. C. Bradley and J. C. de Mello, *Adv. Mater.*, 2011, **23**, 4371–4375.
9 J. J. Liang, L. Li, K. Tong, Z. Ren, W. Hu, X. F. Niu, Y. S. Chen and Q. B. Pei, *ACS Nano*, 2014, **8**, 1590–1600.
10 Z. B. Yu, Q. W. Zhang, L. Li, Q. Chen, X. F. Niu, J. Liu and Q. B. Pei, *Adv. Mater.*, 2011, **23**, 664–668.
11 J. Cui, A. Wang, N. L. Edleman, J. Ni, P. Lee, N. R. Armstrong and T. J. Marks, *Adv. Mater.*, 2001, **13**, 1476–1480.
12 S. L. Ji, W. W. He, K. Wang, Y. X. Ran and C. H. Ye, *Small*, 2014, **10**, 4951–4960.
13 J. Han, S. Yuan, L. Liu, X. Qiu, H. Gong, X. Yang, C. Li, Y. Hao and B. Cao, *J. Mater. Chem. A*, 2015, **3**, 5375–5384.

Published on 31 January 2017. Downloaded by Hefei Institutes of Physical Science, Chinese Academy of Sciences on 7/18/2018 8:29:28 AM.

14 P. Lee, J. Lee, H. Lee, J. Yeo, S. Hong, K. H. Nam, D. Lee, S. S. Lee and S. H. Ko, *Adv. Mater.*, 2012, **24**, 3326–3332.
15 R. M. Rotiso, M. C. Sherrott, A. R. Rathmell, B. J. Wiley and K. I. Winey, *ACS Nano*, 2013, **7**, 7654–7663.
16 G. Khanarian, J. Joo, X. Q. Liu, P. Eastman, D. Werner, K. O'Connell and P. Trefonas, *J. Appl. Phys.*, 2013, **114**, 024302.
17 S. Sorel, P. E. Lyons, S. De, J. C. Dickerson and J. N. Coleman, *Nanotechnology*, 2012, **23**, 185201.
18 S. M. Bergin, Y. H. Chen, A. R. Rathmell, P. Charbonneau, Z. Y. Li and B. J. Wiley, *Nanoscale*, 2012, **4**, 1996–2004.
19 Y. G. Sun, Y. D. Yin, B. T. Mayers, T. Herricks and Y. N. Xia, *Chem. Mater.*, 2002, **14**, 4736–4745.
20 E. J. Lee, M. H. Chang, Y. S. Kim and J. Y. Kim, *Appl. Phys. Lett.*, 2013, **1**, 042118.
21 L. B. Hu, H. S. Kim, J. Y. Lee, P. Peumans and Y. Cui, *ACS Nano*, 2010, **4**, 2955–2963.
22 B. Li, S. R. Ye, I. E. Stewart, S. Alvarez and B. J. Wiley, *Nano Lett.*, 2015, **15**, 6722–6726.
23 R. R. Silva, M. X. Yang, S.-Il. Choi, M. F. Chi, M. Luo, C. Zhang, Z.-Y. Li, P. H. C. Camargo, S. J. L. Ribeiro and Y. N. Xia, *ACS Nano*, 2016, **10**, 7892–7900.
24 A. Tao, P. Sinsermsuksakul and P. D. Yang, *Angew. Chem., Int. Ed.*, 2006, **45**, 4597–4601.
25 K. C. Pradel, K. Sohn and J. X. Huang, *Angew. Chem., Int. Ed.*, 2011, **50**, 3412–3416.
26 L. F. Gou, M. Chipara and J. M. Zaleski, *Chem. Mater.*, 2007, **19**, 1755–1760.
27 S. Koskun, E. S. Ates and H. E. Unalan, *Nanotechnology*, 2013, **24**, 125202.
28 E. J. Lee, Y. H. Kim, D. K. Hwang, W. K. Choi and J. Y. Kim, *RSC Adv.*, 2016, **6**, 11702–11710.
29 T. Kim, A. Canlier, G. H. Kim, J. Choi, M. Park and S. M. Han, *ACS Appl. Mater. Interfaces*, 2013, **5**, 788–794.
30 J. Lee, I. Lee, T. S. Kim and J. Y. Lee, *Small*, 2013, **9**, 2887–2894.
31 T. Kim, A. Canlier, C. Cho, V. Rozyyev and J. Y. Lee, *ACS Appl. Mater. Interfaces*, 2014, **6**, 13527–13534.
32 A. B. V. K. Kumar, C. W. Bae, L. H. Piao and S. H. Kim, *Mater. Res. Bull.*, 2013, **48**, 2944–2949.
33 T. Ariki, J. T. Jiu, M. Nogi, H. Coga, S. Nagao, T. Sugahara and K. Suganuma, *Nano Res.*, 2014, **7**, 236–245.
34 Y. G. Jia, C. Chen, D. Jia, S. X. Li, S. L. Ji and C. H. Ye, *ACS Appl. Mater. Interfaces*, 2016, **8**, 9865–9871.
35 M. Yang, C. M. Neubauer and H. M. Jennings, *Adv. Cem. Based Mater.*, 1997, **5**, 1–7.
36 C. M. Neubauer, M. Yang and H. M. Jennings, *Adv. Cem. Based Mater.*, 1998, **8**, 17–27.
37 S. H. Behrens, D. I. Christl, R. Emmerzael, P. Schurtenberger and M. Borkovec, *Langmuir*, 2000, **16**, 2566–2575.
38 C. J. V. Oss, M. K. Chaudhury and R. J. Good, *Chem. Rev.*, 1988, **88**, 927–941.
39 S. Bhattacharjee and M. Elimelech, *J. Colloid Interface Sci.*, 1997, **193**, 273–285.
40 U. Kreibig and L. Genzel, *Surf. Sci.*, 1985, **156**, 678–700.
41 C. Chen, L. Wang, G. H. Jiang, J. F. Zhou, X. Chen, H. J. Yu and Q. Yang, *Nanotechnology*, 2006, **17**, 3933–3938.
42 M. Park, Y. Sohn, W. G. Shin, J. Lee and S. H. Ko, *Ultrason. Sonochem.*, 2015, **22**, 35–40.
43 H. S. Park and X. H. Qian, *J. Phys. Chem. C*, 2010, **114**, 8741–8748.
44 J. Q. Hu, Q. Chen, Z. X. Xie, G. B. Han, R. H. Wang, B. Ren, Y. Zhang, Z. L. Yang and Z. Q. Tian, *Adv. Funct. Mater.*, 2004, **14**, 183–189.
45 N. Félidj, J. Aubard and J. Lévi, *J. Chem. Phys.*, 1999, **111**, 1195.
46 S. De, T. M. Higgins, P. E. Lyons, E. M. Doherty, P. N. Nirmalraj, W. J. Blau, J. J. Boland and J. N. Coleman, *ACS Nano*, 2009, **3**, 1767–1774.
47 J. van de Groep, P. Spinelli and A. Polman, *Nano Lett.*, 2012, **12**, 3138–3144.

 This journal is © The Royal Society of Chemistry 2017